JOURNAL OF MATERIALS SCIENCE **34** (1999) 3427–3436

Effect of hydrogen and temperature on the resistivity of an aluminum-2 wt % copper thin film

K. S. LEE
Process Research Dept. 4, Semiconductor Research Division, Hyundai Electronics Industries Co., Ltd., P.O. Box 1010, Ichon-si, Kyoungki-do, 467-600, Korea
E-mail: leeks@sr.hei.co.kr

Y. K. LEE
Division of Materials Engineering, School of Applied Science, Nan Yang Technological University, Nan Yang Ave, Singapore 639798
E-mail: asyklee@ntu.edu.sg

Thin metallic films are required to provide interconnection between contacts on devices and between devices. As device dimensions decrease, the low electrical resistivity becomes the most important issue in microelectronics industry. Recently in thin metallic films, hydrogen has been shown to lower the electrical resistivity of thin metallic films, reduce the rate of electromigration in interconnect lines, and lower the stress generated in thin metallic films during annealing. These effects are referred to as hydrogen effects. Low temperature resistivity measurements were performed to determine the effect of hydrogen and temperature on the resistivity of an aluminum-2 wt % copper film. Low temperature control experiments were performed in helium since it has a similar thermal conductivity as hydrogen but is chemically inert. The electrical resistivity of an aluminum-2 wt % copper alloy is lowered by hydrogen even at low temperature. The temperature coefficient of resistivity (TCR) values are identical within the experimental error (± 0.005 $\mu\Omega$ cm/K). This means that phonon scattering is identical. So the decrease of the electrical resistivity is due to the decrease in the residual resistivity. Hydrogen effects are reversible for an aluminum-2 wt % copper alloy at room temperature because the adsorption and desorption of hydrogen occur. Hydrogen effects are slowly reversible for an aluminum-2 wt % copper alloy at low temperature because the adsorption of hydrogen occurs, but the desorption of hydrogen does not occur readily.

1. Introduction

Thin metallic films are required to provide interconnection between contacts on devices and between devices and the outside world [1]. The application of metals and metal-like layers is called metallization [2]. The metallization applications can be divided into two groups: (i) gate and interconnection and (ii) contact. The interconnection metallization is generally the same as the gate metallization. All metallizations involving direct contact with the semiconductor surface are called contact metallizations. Aluminum is used as the contact metal for devices and also as a second-level connection to the outside world [3]. Aluminum has most of the desired properties of the metallization including its low resistivity, its ease of processing, and its good adherence to the semiconductor surface. As device dimensions decrease, the electrical resistivity becomes the most important issue in microelectronics industry.

The low electrical resistivity film has better electromigration resistance. Electromigration is the mass transport of positive metal ions under the driving force of a high current density [4]. The electromigration atomic flux is driven by an electric field that is modified by an electron wind force. Continuing advances in the fields of ultra-large-scale integration (ULSI), and the continued development of smaller and smaller devices **have** aroused concern about existing metallization schemes and the reliability of aluminum and its alloys as a current carrier. As device dimensions decrease, electromigration becomes one of the most important issues. An important feature of the electromigration is that the mass flux is directly proportional to the electrical resistivity of the thin metallic film. As the electrical resistivity of the thin metallic film decreases, the rate of electromigration decreases proportionally. The low electrical resistivity has another merit. The characteristics of metal-oxide-semiconductor devices depend on several parameters, of which the *RC* time constant is the most important. The higher the *RC* value, the slower is the operating speed of the device. The *R* and *C* are,

respectively, the effective total resistance and capacitance of the device at the gate and interconnection level [5, 6].

Since the electrical resistivity is a measure of defect density at a given temperature, the low resistivity film has fewer defects. In other words, the low resistivity films are **good** and reliable films. Heat generation due to high resistivity is another problem in current microelectronics industry. As the feature size decreases, the current density increases. Heat generation is the cause of temperature rise in the material and its surroundings, which receives the dissipated energy. This problem can be solved by lowering the electrical resistivity. For these reasons, the research to produce low resistivity films has been continued. *Since the electrical resistivity is a material property* [7], *the low resistivity material must be considered in order to produce low resistivity films*. Recently copper, as the inter-level metal, has drawn considerable attention [8]. Copper offers low electrical resistivity, high heat capacity, high density, high thermal conductivity, and high electromigration resistance. It is easily sputtered or electroplated. However, there are presently three major problems with copper that need be solved. They are related to its poor bonding to the SiO_2 surface, its poor corrosion resistance, and dry etching that appears to be very difficult [9].

Reducing the temperature is seen as a possible means to improve device performance because it lowers the resistance of interconnecting materials [10, 11]. *The experimental data available indicate about an order of magnitude reduction of resistance of aluminum lines of the type used in integrated circuits* [12–14].

Gaseous hydrogen has been shown to affect the electrical and mechanical properties of thin metallic films [15]. The mechanical effects have been reported in the first half of the 20th century as hydrogen embrittlement. In hydrogen embrittlement, hydrogen was found to lower the failure strength of various metals and normally caused a change in fracture mode from transgranular to intergranular [16]. Recently in thin metallic films, the presence of hydrogen led to improvements in electrical and mechanical properties of thin metallic films. Hydrogen has been shown to lower the electrical resistivity of thin metallic films, reduce the rate of electromigration in interconnect lines [17], and lower the stress generated in thin metallic films during annealing [18]. For this paper, these effects will be referred to as hydrogen effects [19]. Until now, hydrogen effects have been studied in the range of room temperature and above. This was partially due to the temperature at which the samples were deposited, and partially due to the system used to measure the electrical resistivity. But, in this report, hydrogen effects at cryogenic temperatures were studied for possible cryogenic temperature microelectronics applications.

2. Experimental

2.1. Sample preparation

Every sample was fabricated at IBM. The test vehicle used for these experiments was defined using standard photolithographic techniques. The conductor stripes were aluminum-2 wt % copper alloy. The conductor stripes were 3 μm wide, 800 nm thick and 250 μm in length. Three parallel conductor stripes were deposited with a spacing of 5 μm. The conductor stripes were E-beam evaporated onto a flat oxidized silicon wafer. The substrate temperature during E-beam evaporation was 413–423 K. Following deposition, the samples were annealed at 673 K for 1 hour to stabilize the grain structures.

The samples were mounted on 28-pin dual-in-line ceramic packages with conductive silver paste. The 28-pin dual-in-line ceramic packages were not vacuum ready in the as-received state. A three step process was used to clean the packages for use in vacuum. First, the packages were rinsed in acetone and wiped with lint-free paper to remove any gross organic contaminants. After wiping the packages thoroughly, the packages were rinsed in acetone again. Because acetone left behind a water residue when it evaporated, the packages were placed in an isopropyl alcohol (IPA) bath immediately after rinsing with acetone a second time. The IPA bath was then placed in an ultrasonic cleaner for 20 min. The cleaned packages were then dried by blowing nitrogen over them. The packages then placed in a covered carrier until they were used in experiments.

2.2. Vacuum system

Fig. 1 shows a schematic for the high vacuum system used for low temperature experiments. The high vacuum system consisted of a rotary oil-sealed mechanical pump, a cryosorption roughing pump, and a sputter ion pump. The Varian 'Vac-Sorb' cryosorption pump was baked out before every evacuation. Typically a bake-out of the cryosorption pump at 440 K for 24 hours

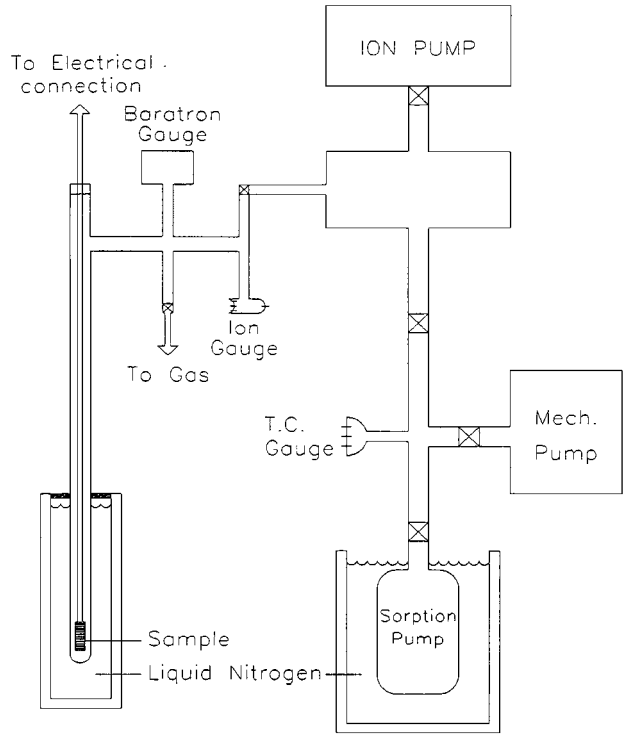

Figure 1 A schematic for the high vacuum system used for low temperature experiments.

allowed for pressures in the 9×10^{-5} Torr range to be reached in the vacuum chamber before opening the gate valve of the main ion pump. During the bake-out, a 'Welch duo-seal' mechanical pump was used to pump out the desorbed gases from the synthetic Zeolite in the cryosorption pump. Low vacuum pressure in the vacuum chamber was measured by the MKS type 222BA-01000CB Baratron gauge. The Baratron gauge range was 0–1000 Torr. The roughing line pressure was measured by the Huntington Model 1518 thermocouple gauge. The thermocouple gauge range was 0–1000 microns of mercury. High **vacuum pressure in the vacuum pressure** was measured by the Huntington IP-100 Bayard Alpert ion gauge. The Varian VacIon pump has a pumping speed of 220 l/s. A vacuum chamber pressure of 1×10^{-7} Torr was achieved with a 42-hour pumping by the ion pump.

A special shaped vacuum chamber was designed to do low temperature experiments. The MDC GA-075P-S 304 stainless steel to 7740 Pyrex adapter was used to attach a 20-in. long Pyrex tube. The glass-to-metal adapter and the glass tube were attached by the glass blowing and annealing technique. The Aladdin Cryogenic Dewar was installed around the long glass tube to contain liquid nitrogen. The Styrofoam cover was installed to minimize the liquid nitrogen loss. Ultra high purity grade hydrogen, helium, and nitrogen gas cylinders were connected through the Granville-Phillips Series 203 Variable Leak valve. Hydrogen gas and helium gas were used to determine hydrogen effects. Nitrogen gas was used to break the vacuum.

2.3. Low temperature measurements

Off package contacts were made to make electrical connections to the constant current source and the digital multimeter. Fig. 2 shows the electrical wiring schematic for the low temperature experiments. A 9.5 mm diameter copper wire was wrapped around the appropriate pin of the 28-pin dual-in-line ceramic packages. The wire and pin were then pinched with a pair of pliers. Each pin with the wrapped wire was soldered with indium to secure electrical contacts. Four wires were connected through the four-hole alumina tube to make electrical isolation between wires. The wire through the alumina tube was wrapped around the appropriate pin of the 8-pin electrical feedthroughs. The pin of the 8-pin feedthroughs was bent to have mechanical strength. Each pin of the electrical feedthroughs was soldered with indium to make sure electrical contacts. The pins of the electrical feedthroughs were electrically isolated by alumina beads. The alumina tube and alumina beads were cleaned in a manner similar to that used in the 28-pin dual-in-line ceramic packages. The temperature of the sample was measured by the OMEGA type 1PT100-K82 platinum resistance temperature detector (RTD) element. The 100 Ω platinum RTD element was attached by an alligator clip to ensure physical contact. As shown in Fig. 2, two separate 9.5 mm diameter copper wires of the same length were attached to each pin of the platinum RTD element by indium soldering. The wire isolation and the 8-pin electrical feedthroughs connection were similar to that used in current and voltage connections. Keithley Model 227 constant current source (I in Fig. 2) and Keithley Model 195A digital multimeters (one for V and the other for T in Fig. 2) were connected to the appropriate pins of the 8-pin electrical feedthroughs. The current setting was 100 μA with a total accuracy of ± 1.7 μA. The DC voltage range was 20 mV with a resolution of 100 nV. The temperature span was from 73 to 503 K with a resolution of 0.01 K. The voltage and temperature readings from digital multimeters were recorded to an IBM XT personal computer via IEEE-488 computer interfaces. All data were stored on the hard disk. Data were taken once a minute.

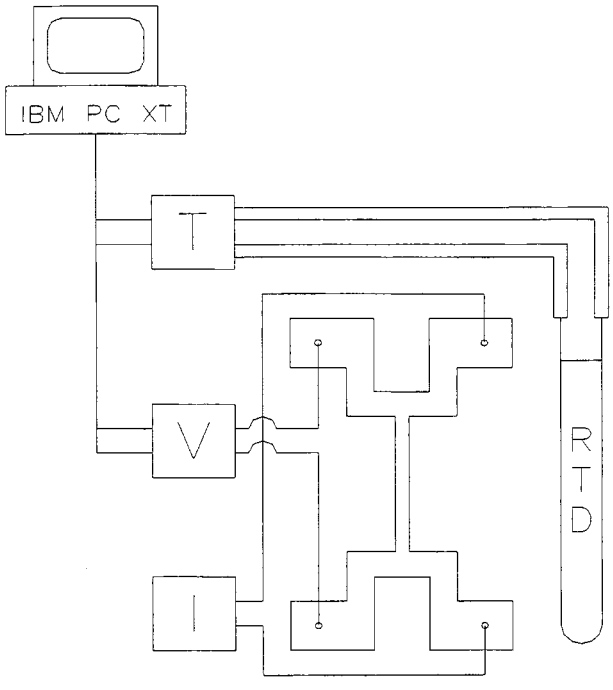

Figure 2 The electrical wring schematic for the low temperature experiments.

3. Results and discussion

Resistivity of a metal is a function of solute concentration, defect concentration and temperature. Since the same film was used, the solute concentration is not a variable. The goal of these experiments is then to determine the effect of hydrogen and temperature on the resistivity of an aluminum-2 wt % copper film.

In these experiments, the metal film is held in the center of a 19 mm diameter glass tube (see Fig. 1). The glass tube is then surrounded with liquid nitrogen. Surprisingly the steady state difference in temperature (ΔT) between the liquid nitrogen and the sample was 100 K when the glass tube was evacuated ($\sim 10^{-7}$ Torr). The temperature differences in hydrogen ($\sim$30 Torr) and helium ($\sim$30 Torr) were 5 and 10 K respectively. In all cases, therefore, the temperature of the film, as measured by the RTD, was reported.

Fig. 3 shows the time-dependent resistivity and temperature change of the aluminum-2 wt % copper alloy. Only steady state values are considered. The resistivity and temperature data were taken simultaneously. The

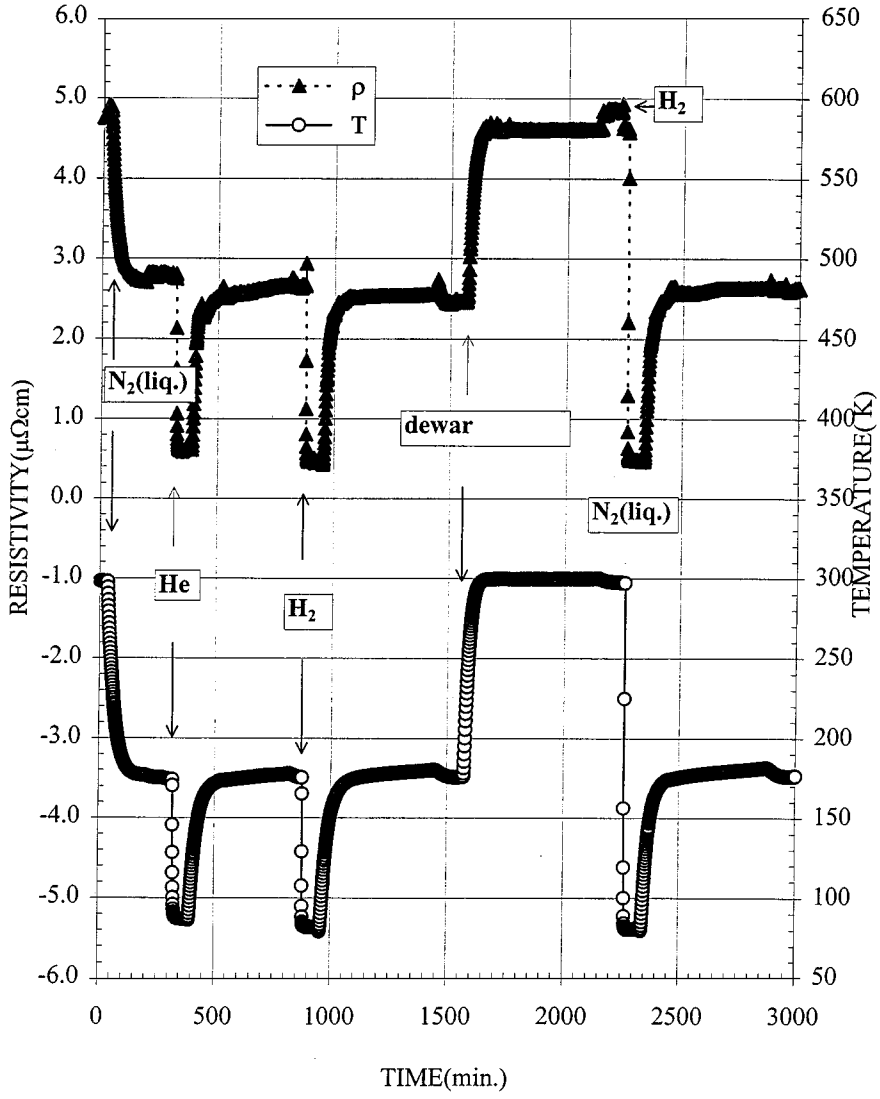

Figure 3 The time-dependent resistivity and temperature change of the aluminum-2 wt % copper alloy.

top curve (filled triangles) is the resistivity ($\mu\Omega$ cm) using the ordinate on the left. The bottom curve (open circles) is the temperature (K) using the ordinate on the right. Before the liquid nitrogen addition at the 34th min, the chamber pressure was 1.1×10^{-7} Torr, and the sample resistivity was 4.90 $\mu\Omega$ cm at 298 K. After steady state was reached, ultra-high-purity grade helium gas was introduced at the 320th min. Fig. 4 details the time-dependent resistivity and temperature change of the aluminum-2 wt % copper alloy due to the helium introduction. Before the helium introduction, the chamber pressure was 1.3×10^{-7} Torr, and the sample resistivity was 2.77 $\mu\Omega$ cm at 174 K. After the helium introduction, the chamber pressure was 28 Torr and the sample resistivity was 0.628 $\mu\Omega$ cm at 87 K. After steady state was reached, the helium was evacuated at the 390th min. After evacuation, the chamber pressure was 1.4×10^{-7} Torr and the sample resistivity was 2.67 $\mu\Omega$ cm at 175 K. Ultra-high-purity grade hydrogen gas was introduced then at the 874th min. Fig. 5 details the time-dependent resistivity and temperature change of the aluminum-2 wt % copper alloy due to hydrogen introduction. After the hydrogen introduction, the chamber pressure was 30 Torr and the sample resistivity was 0.458 $\mu\Omega$ cm at 82 K. After steady state was reached, the hydrogen was evacuated at the 950th min. After steady state was reached, a dewar was removed at the 1569th min. Before the dewar removal, the chamber pressure was 1.2×10^{-7} Torr and the sample resistivity was 2.47 $\mu\Omega$ cm at 176 K. At this temperature ultra-high-purity grade hydrogen gas was introduced at the 2231st min. Fig. 6 details the time-dependent resistivity and temperature change of the aluminum-2 wt % copper alloy due to the hydrogen introduction at 298 K. Before the hydrogen introduction, the chamber pressure was 1.1×10^{-7} Torr and the sample resistivity was 4.84 $\mu\Omega$ cm at 298 K. After the hydrogen introduction, the chamber pressure was 27 Torr and the sample resistivity was 4.64 $\mu\Omega$ cm at 297 K. After this steady state, the dewar was installed again and liquid nitrogen was added at the 2259th min. After the liquid nitrogen addition, the chamber pressure was 21 Torr and the sample resistivity was 0.475 $\mu\Omega$ cm at 81 K. After this steady state, the hydrogen gas was evacuated at the 2335th min. Table I shows the average steady state data in the experiment sequence. Column 2–5 shows the values in parenthesis when the entire experiments were repeated. From Fig. 3 and Table I, one can notice that the hydrogen effect is reversible (see stage numbers 1 and 7). In other words, the electrical resistivity is lowered only

TABLE I Average steady state data in experimental sequence

Stage number	Temperature (K)	ρ ($\mu\Omega$ cm)	TCR ($\mu\Omega$ cm/K)	Chamber pressure (Torr)
1	298(297)	4.90(5.35)	N/A	Vacuum $1.1(1.5) \times 10^{-7}$
2	174(177)	2.77(2.20)	0.017(0.026)	Vacuum $1.3(1.4) \times 10^{-7}$
3	87(85)	0.628(0.488)	0.025(0.019)	Helium $2.8(3.0) \times 10^{1}$
4	175(177)	2.67(2.10)	0.023(0.018)	Vacuum $1.4(1.2) \times 10^{-7}$
5	82(81)	0.458(0.394)	0.024(0.018)	Hydrogen $3.0(3.0) \times 10^{1}$
6	176(184)	2.47(2.31)	0.022(0.019)	Vacuum $1.2(2.1) \times 10^{-7}$
7	298(297)	4.84(5.24)	0.019(0.026)	Vacuum $1.1(1.6) \times 10^{-7}$
8	297(296)	4.64(4.92)	N/A	Hydrogen $2.7(3.5) \times 10^{1}$
9	81(80)	0.475(0.404)	0.019(0.021)	Hydrogen $2.1(2.6) \times 10^{1}$
10	177(178)	2.69(2.14)	0.023(0.018)	Vacuum $1.8(15) \times 10^{-7}$

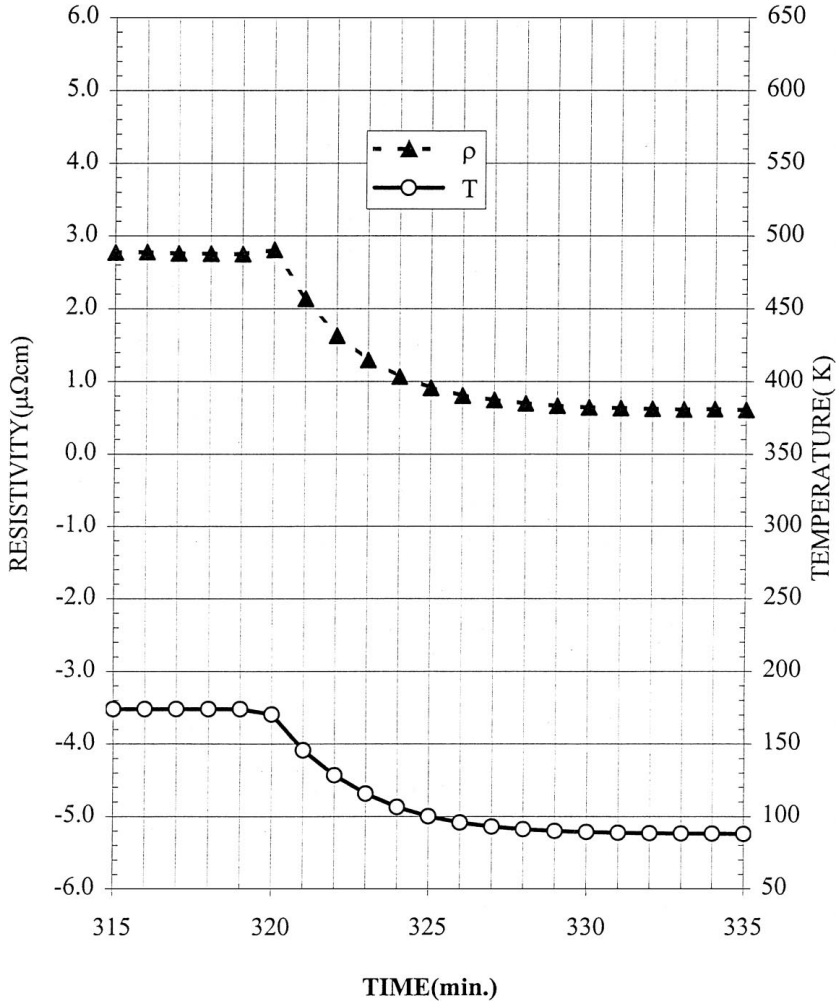

Figure 4 The time-dependent resistivity and temperature change of the aluminum-2 wt % copper alloy due to the helium introduction.

in the presence of hydrogen. Low temperature control experiments were performed in helium since it has a similar thermal conductivity [20] as hydrogen but is chemically inert.

The measured resistivity ρ_T is generally a function of temperature, but on approaching absolute zero it comes to assume a constant residual value, known as the residual resistivity ρ_0. The quantity ρ_0 arises from the presence of impurities, defects, and strains in the metal lattice. Subtraction of ρ_0 from the measured resistivity gives a value of the resistivity appropriate for a perfectly pure, strain-free specimen. The temperature-dependent resistivity obtained is called the ideal or intrinsic resistivity. It is designated by ρ_{iT} at temperature T, and it is caused by the interactions of the conduction electrons with the thermal vibrations of the ions of the lattice [21]. The separation of the total resistivity ρ_T into temperature-dependent (ρ_{iT}) and temperature-independent (ρ_0) contributions in this way is known as Matthiessen's rule [22], which may be written as follows.

$$\rho_T = \rho_0 + \rho_{iT} \tag{1}$$

Matthiessen's original statement was to the effect that the increase in resistance due to a small concentration of another metal in solid solution is, in general, independent of the temperature. This is equivalent to saying

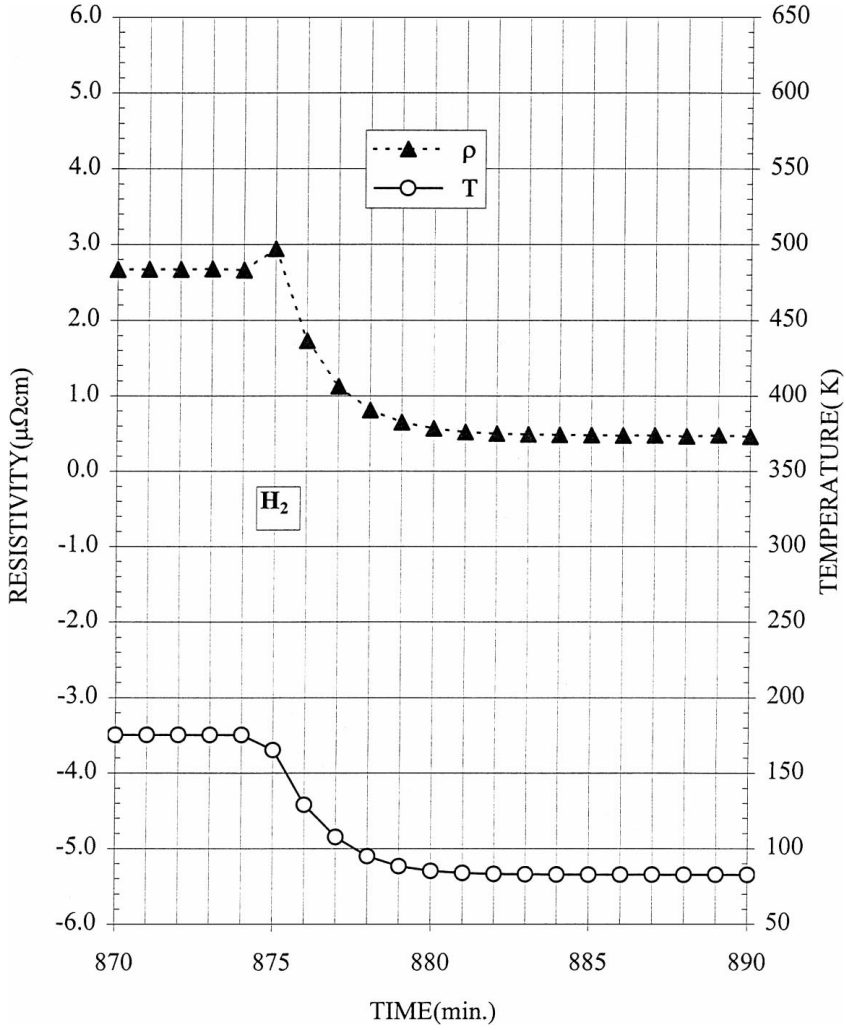

Figure 5 The time-dependent resistivity and temperature change of the aluminum-2 wt % copper alloy due to the hydrogen introduction.

that the addition of small amounts of impurity atoms does not modify the thermal vibrations of the ions of the host lattice, so that the impurity contribution to the resistivity may be considered apart from the ideal or thermal contribution. As described above, helium was used to prove hydrogen effects at low temperature. From Table I, Figs 4, and 5, stage 3 and stage 5 are comparable. At stage 3, the electrical resistivity at 87 K in helium ($\rho_{87\,\mathrm{K,\,He}}$) was 0.628 $\mu\Omega$ cm. At stage 5, the electrical resistivity at 82 K in hydrogen ($\rho_{82\,\mathrm{K,\,H_2}}$) was 0.458 $\mu\Omega$ cm. Because of the temperature difference, the electrical resistivities should be corrected to compare as follows. If Equation 1 is rewritten for $\rho_{T,\,\mathrm{He}}$, ρ_0 can be replaced by the electrical resistivity due to helium and defects etc. ρ_{He} and ρ_{iT} can be replaced by the recommended electrical resistivity [23] of the aluminum-2 wt % copper alloy at T ($\rho_{T,R}$). The recommended values are for well-annealed high-purity specimens of aluminum-2 wt % copper alloys.

Therefore,

$$\rho_{T,\,\mathrm{He}} = \rho_{\mathrm{He}} + \rho_{T,\,R} \tag{2}$$

Similarly,

$$\rho_{T,\,\mathrm{H_2}} = \rho_{\mathrm{H_2}} + \rho_{T,\,R} \tag{3}$$

where $\rho_{\mathrm{H_2}}$ is the electrical resistivity due to hydrogen and defects, etc. The other conditions were the same because the sample was same. The only difference was helium or hydrogen. From the recommended electrical resistivity, $\rho_{87\,\mathrm{K},R}$ and $\rho_{82\,\mathrm{K},R}$ were calculated by the interpolation method.

$$\rho_{87\,\mathrm{K},\,R} = 0.491\ \mu\Omega\ \mathrm{cm} \tag{4}$$

$$\rho_{82\,\mathrm{K},\,R} = 0.444\ \mu\Omega\ \mathrm{cm} \tag{5}$$

From Equations 2 and 4,

$$\rho_{87\,\mathrm{K,\,He}} = \rho_{\mathrm{He}} + 0.491\ \mu\Omega\ \mathrm{cm} \tag{6}$$

$$0.628\ \mu\Omega\ \mathrm{cm} = \rho_{\mathrm{He}} + 0.491\ \mu\Omega\ \mathrm{cm} \tag{7}$$

$$\rho_{\mathrm{He}} = 0.137\ \mu\Omega\ \mathrm{cm} \tag{8}$$

From Equations 2, 5, and 8,

$$\rho_{82\,\mathrm{K,\,He}} = 0.137\ \mu\Omega\ \mathrm{cm} + 0.444\ \mu\Omega\ \mathrm{cm} \tag{9}$$

$$\rho_{82\,\mathrm{K,\,He}} = 0.581\ \mu\Omega\ \mathrm{cm} \tag{10}$$

$\rho_{82\,\mathrm{K,\,H_2}}$ ($= 0.458 \pm 0.023\ \mu\Omega$ cm) is considerably lower than $\rho_{82\,\mathrm{K,\,He}}$ ($= 0.581 \pm 0.029\ \mu\Omega$ cm). In other words, the electrical resistivity of an aluminum-2 wt % copper alloy is lowered by hydrogen in the presence of hydrogen. The measurements of the electric resistivity of thin metallic films can give valuable data on the type

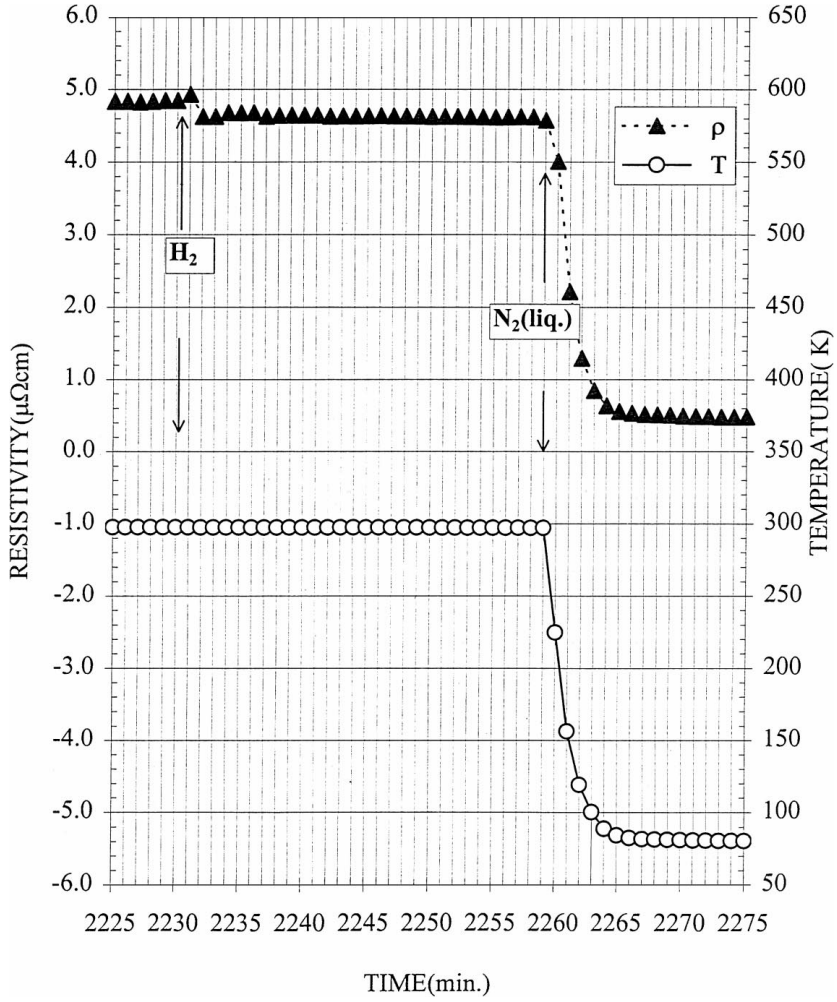

Figure 6 The time-dependent resistivity and temperature change of the aluminum-2 wt % copper alloy due to the hydrogen introduction at 298 K.

of electronic interactions. The temperature coefficient of resistivity (TCR) is defined as follows.

$$\mathrm{TCR} = \Delta\rho/\Delta T \tag{11}$$

From the average steady state data (Table I), TCR values between stages were calculated. The calculated values between stages are shown in Table I. TCR values are identical within the experimental error ($\pm 0.005\ \mu\Omega$ cm/K). These indicate that the slopes of resistivity versus temperature graphs are identical. These facts can be explained as follows. In dilute alloys, the residual resistivity (ρ_0) is expected to vary linearly with solute concentration. This rflects the fact that the scattering from each impurity atom should be independent of the others so that the total scattering is just proportional to the number of scatterers, i.e. to the solute concentration. The word 'scattering' applied to electron waves has the same sort of meaning as 'collisions' applied to electrons regarded as particles [24]. The residual resistivity (ρ_0) caused by a concentration x of solute atoms in the solvent metal, may be described by Nordheim's concentration rule [25] in the form

$$\rho_0 \propto x(1-x) \tag{12}$$

from which it is seen that for small x, ρ_0 is proportional to x. In practice, it is usually assumed that alloys containing less than about one atomic percent of solute atoms can be treated as dilute. In addition to scattering by solute atoms, residual scattering can arise from physical defects. Matthiessen's rule implies that the temperature-independent resistivity (ρ_0) is effectively in series with the temperature-dependent part (ρ_{iT}). ρ_{iT} is known variously as the thermal, the ideal, the intrinsic, the lattice, or the phonon resistivity. The phonon may be defined as a single quantum of the quantized energies of the lattice vibrations [21]. Suppose that the scattering of electrons by the solute atom can be described by a relaxation time τ_0 [24]. Then at very low temperatures when the scattering of electrons by phonons is effectively dead, ρ_0 is given by

$$\rho_0 = m/ne^2\tau_0 \tag{13}$$

where n is the number of electrons per unit volume and m and e are their mass and charge. If at a high temperature T, when the scattering of electrons by phonons is dominant, ρ_{iT} is given by

$$\rho_{iT} = m/ne^2\tau_{iT} \tag{14}$$

where τ_{iT} is the relaxation time due to phonon scattering. Now consider an alloy at temperature T when both impurity scattering (solute atoms) and phonon

scattering operate together. The relaxation time τ for both processes is given by

$$1/\tau = 1/\tau_0 + 1/\tau_{iT} \tag{15}$$

This holds if the two scattering operate independently; since the probability of scattering is inversely proportional to the corresponding relaxation time, this expression is equivalent to adding the probabilities of scattering by the two separate mechanisms. One can truly split the phonon scattering and the impurity scattering at liquid helium (4.2 K) or lower temperatures. However, the experimental apparatus used in this work did not allow the achievement of these low temperatures. The resistivity of the alloy at temperature T (ρ_T) is related to by the expression

$$\rho_T = m/ne^2\tau \tag{16}$$

By combining Equations 13–16, one gets the Matthiessen's rule.

$$\rho_T = \rho_0 + \rho_{iT} \tag{17}$$

Fig. 7 [23] shows that the resistivities of aluminum-copper alloy increases with increasing amount of solute concentration. The slope of the individual ρ_T versus T lines remain constant above 80 K. In this temperature range, increasing solute concentrations merely cause a linear shift of the ρ_T versus T curves to higher resistivity values in accordance with Matthiessen's rule. From the results, the electrical resistivity of the film was lowered in the presence of hydrogen. In all cases, TCR values are identical within the experimental error ($\pm 0.005\ \mu\Omega$ cm/K). This means that phonon scattering is identical in all cases. So the decrease of the electrical resistivity by hydrogen is due to the decrease in the residual resistivity. The number of impurity atoms is generally constant in a given metal or alloy [26]. Since the same film was used, the solute concentration is identical. So the decrease of the electrical resistivity by hydrogen is due to the decrease in the residual resistivity. The possible mechanism of the decrease in electrical resistivity by hydrogen must be the decrease of the defect density and the interactions between hydrogen atoms and host metal atoms. If an electric field influences polarizable free gas molecules, their electric equilibrium will be disturbed, and their electron clouds will be shifted with respect to their positive charges. The same phenomenon is to be expected if such molecules enter the electric field of a phase boundary, for example, if they are adsorbed on an ionic lattice or a metal surface [27]. The electric field at a metal surface is the

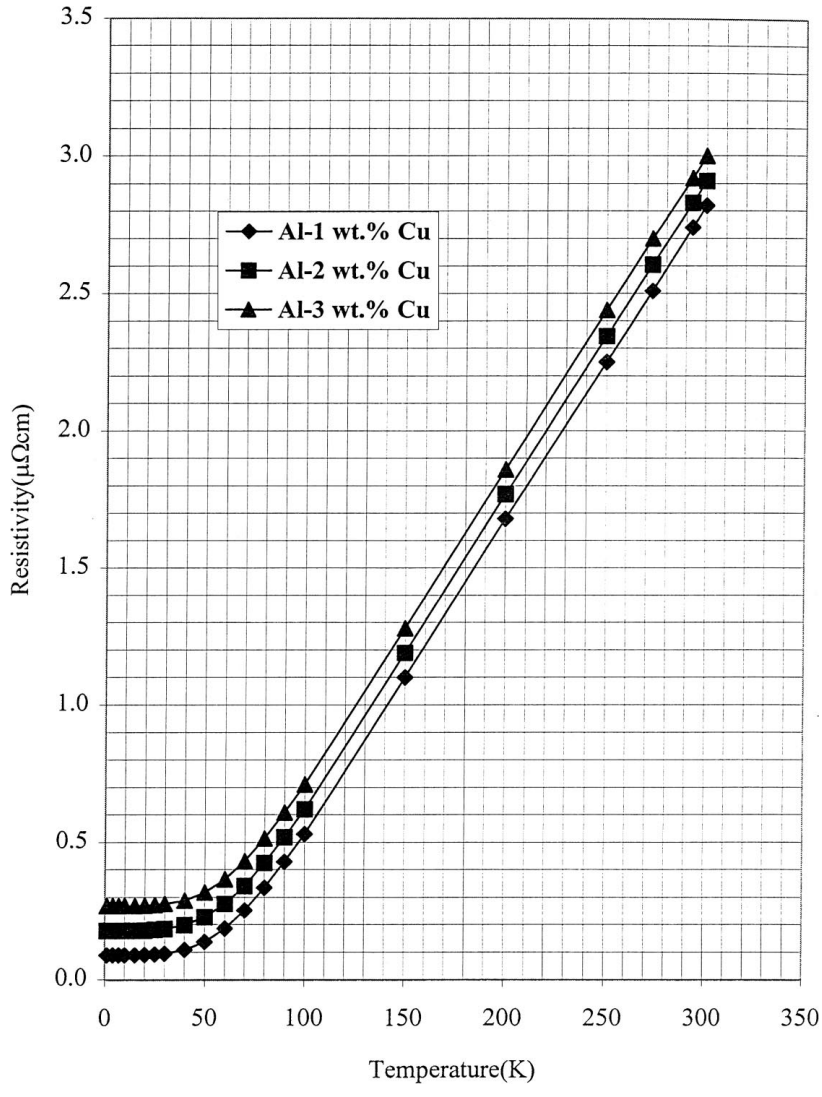

Figure 7 The recommended electrical resistivity as a function of temperature for aluminum-copper alloys.

origin of work function $e\phi$ of escaping electrons. The potential ϕ which must be overcome is at the same time a measure of the electron affinity of the metal surface. The observed decrease or increase of the work function of metal surfaces on adsorption of foreign molecules is to be expected if only an electron shift occurs to or from the film surface. If the electrons of the adsorbed molecules become part of the metal electron gas, or if the metal electrons of the adsorbed molecules become part of the shells of the molecule, not only a change of the work function, in addition, a change of the electrical resistance of the metal will be observed.

The effect of hydrogen is not completely reversible at low temperature (175 K). Consider stages 2, 4 and 6. Between stages 2 and 4, helium had been introduced and removed. The resistivity recovered to within 0.1 $\mu\Omega$ cm. Hydrogen was then introduced and removed. The resistivity did not completely recover, i.e. it remained lower by $\sim$0.25 $\mu\Omega$ cm (0.28 Ω). When the system was evacuated and returned to room temperature (stage 7), the hydrogen effect vanished ($\Delta\rho = 0.06$ $\mu\Omega$ cm between stages 1 and 7). The same phenomena have been reported [27]. In that study hydrogen was adsorbed on nickel films at 90 K and a hydrogen pressure of 10^{-3} Torr. After evacuation to 10^{-6} Torr, the resistance change was 0.3 Ω. The adsorption of hydrogen occur by the same mechanism at liquid nitrogen temperature (77 K) as it does at room temperature. The desorption of hydrogen occurs at room temperature, but this desorption does not occur at 77 K [28]. This can be explained by the interactions between hydrogen and lattice defects. Hydrogen tends to form an impurity-defect complex in a metal lattice [29]. As the size of the complex increased, that is, as more hydrogen atoms became associated with each defect, the binding energy of the hydrogen to the defect decreased. Due to the lower binding energy, the density of scattering state electrons decreased and lowered the effective scattering cross-section of the complex. Hydrogen also tends to diffuse to traps such as defects [30]. Trapping of hydrogen at defects can lead to anomalously low diffusion coefficients [31]. Hydrogen does not enter a defect, because hydrogen moves to stable interstitial sites in the vicinity of a defect, where it would complex to the defect [32, 33].

In summary, hydrogen lowers the effective defect density by several mechanisms as described above. The effects of hydrogen on the electrical resistivity are linked to the effects of hydrogen on the effective defect density. In this case, hydrogen effects are reversible at room temperature because the interactions between hydrogen and lattice defects are limited to the surface and near surface region, and the adsorption and desorption of hydrogen occur. Hydrogen effects are irreversible at low temperature because the adsorption of hydrogen occurs, but the desorption of hydrogen does not occur readily.

4. Conclusions

Low temperature resistivity measurements were performed to determine the effect of hydrogen and temperature on the resistivity of an aluminum-2 wt % copper film. The resistivity and temperature data were taken simultaneously. Low temperature control experiments were performed in helium since it has a similar thermal conductivity as hydrogen but is chemically inert. Based upon these experiments and the subsequent analysis, the following conclusions were drawn:

1. The electrical resistivity of an aluminum-2 wt % copper alloy is lowered by hydrogen even at low temperature. The decrease of the electrical resistivity for an aluminum-2 wt % copper alloy by hydrogen is due to the decrease in the residual resistivity.
2. The temperature coefficient of resistivity (TCR) values are identical within the experimental error ($\pm$0.005 $\mu\Omega$ cm/K). This means that phonon scattering is identical in all cases. So the decrease of the electrical resistivity for an aluminum-2 wt % copper alloy by hydrogen is due to the decrease in the residual resistivity.
3. Hydrogen effects are reversible for an aluminum-2 wt % copper alloy at room temperature because the interactions between hydrogen and lattice defects are limited to the surface and near surface region, and the adsorption and desorption of hydrogen occur.
4. Hydrogen effects are slowly reversible for an aluminum-2 wt % copper alloy at low temperature because the adsorption of hydrogen occurs, but the desorption of hydrogen does not occur readily.

References

1. S. SZE, "VLSI Technology" (McGraw Hill, NY, 1988) p. 375.
2. S. MURARKA, "Metallization: Theory and Practice for VLSI and ULSI" (Butterworth-Heinemann, MA, 1993).
3. A. MILNES and D. FEUCHT, "Heterojunctions and Metal-Semiconductor" (Academic Press, NY, 1972).
4. K. RODBELL, PhD thesis, Rensselaer Polytechnic Institute, Troy, NY, 1986.
5. H. HUNTINGTON and A. GRONE, *J. Phys. Chem. Solids* **20**(76) (1961).
6. S. MURARKA and M. PECKERAR, "Electronic Materials Science and Technology" (Academic Press, CA, 1989).
7. J. SHACKELFORD, Introduction to Materials Science for Engineers (MacMillan Publishing, NY, 1988).
8. T. OHMI, T. SAITO and T. SHIBATA, in Proc. 5th Int. IEEE VLSI Multilevel Interconnection Conf. IEEE Cat. # 88CH 2624–2625 (IEEE, NY, 1988) p. 135.
9. R. GUTMANN, T. CHOW, W. GILL, A. KALOYEROS, W. LANFORD and S. MURARKA, *Mater. Res. Soc. Symp. Proc.* **337** (1994) 41.
10. P. SOLOMON, *Proc. IEEE* **70**(1) (1982) 489.
11. R. KEYES, E. HARRIS and K. KONNERTH, *Proc. IEEE* **58**(12) (1970) 1914.
12. F. GAENSSLEN, V. RIDEOUT, E. WALKER and J. WALKER, *IEEE Transactions on Electron Devices* **ED-24** (1977) 218.
13. W. DUMKE, *ibid.* **ED-28**(5) (1981) 494.
14. B. LENGELER, *Cryogenics* **14** (1974) 439.
15. C. APBLETT, D. MUIRA, M. SULLIVAN and P. FICALORA, *J. Appl. Phys.* **10**(71) (1992) 4926.
16. B. WILCOX and G. SMITH, *Acta Metall.* **13** (1965) 331.
17. K. RODBELL and P. FICALORA, *J. Appl. Phys.* **65**(8) (1989) 3107.
18. C. APBLETT and P. FICALORA, *ibid.* **69**(8) (1991) 4431.
19. C. APBLETT, PhD thesis, Rensselaer Polytechnic Institute, Troy, NY, 1992.
20. Y. TOULOUKIAN, P. LILEY and S. SAXENA, "Thermal Conductivity" (Plenum Press, NY, 1970).

21. G. MEADEN, "The Electrical Resistance of Metals" (Plenum Press, NY, 1965).
22. A. MATTHIESSEN, *Rep. British Assoc.* **32** (1862) 144.
23. C. HO *et al. J. Phys. Chem. Ref. Data* **12**(2) (1983) 183.
24. J. DUGDALE, "The Electrical Properties of Metals and Alloys" (Edward Arnold, London, 1977).
25. L. NORDHEIM, *Ann. Physik* **9**(5) (1931) 607.
26. E. HUMMEL, "Electronic Properties of Materials" (Springer-Verlag, NY, 1985).
27. R. SUHRMANN, *Adv. Catalysis*, **7** (1955) 303.
28. P. SELWOOD, *J. Amer. Chem. Soc.* **78** (1955) 697.
29. L. YONGMING, G. BINGLIN, G. NAIFEI, X. JIAJIONG, C. BISONG and Y. WEIZHONG, *Chinese Physics* **2**(9) (1989) 334.
30. P. RICHARDS and S. MYERS, *J. Chem. Phys.* **92**(3) (1990) 1972.
31. K. YANG, M. CAO, X. WAN and C. SHI, *Scr. Metall.* **23** (1989) 203.
32. R. WISTROM, P. BORGESEN, L. SASS, B. NIELSEN, T. LEUNG and K. LYNN, *J. Appl. Phys.* **70**(12) (1991) 7349.
33. J. BUGEAT and E. LIGEON, *Phys. Lett. 1* **71A** (1979) 93.

Received 14 July
and accepted 24 November 1998